Advanced Materials Research *Online: 2011-07-04*
ISSN: 1662-8985, Vol. 278, pp 174-179
doi:10.4028/www.scientific.net/AMR.278.174
© 2011 The Author(s). Published by Trans Tech Publications Ltd, Switzerland.

On The Oxidation Resistance of Nickel-Based Superalloys

Atsushi Sato[1,a], Johan J Moverare[2,b], Magnus Hasselqvist[2,c] and Roger C Reed[1,d]

[1]Depertment of Metallurgy and Materials, University of Birmingham, U.K.

[2]Finspång, Siemens Industrial Turbomachinery AB, Sweden

[a]axs756@bham.ac.uk, [b]johan.moverare@siemens.com, [c]magnus.hasselqvist@siemens.com, [d]r.c.reed@bham.ac.uk

Key words: Nickel alloys, Oxidation, Oxide, Thermodynamics, Segregation

Abstract. In this paper, the factors influencing the oxidation resistance of superalloys are studied. A model is proposed by which the Al_2O_3-forming properties of a given composition can be estimated, based upon the thermodynamic and kinetic factors influencing scale growth. The numerical modelling is tested by experimental work on a number of compositional variants of the newly-developed SCA425+ superalloy, which contains appreciable quantities of Cr. The modelling is shown to be in broad agreement with experiment. The effects of Al, Cr and Si on the oxidation resistance of this class of alloy have been rationalised.

Introduction

Most existing nickel-based superalloys have been designed for aeroengine applications; experience has shown that they are not ideal for use in industrial gas turbines (IGTs) of the type used for power generation, on account of their inadequate resistance to environmental degradation. An accurate model which allows the oxidation resistance of nickel-based superalloys to be estimated as a function of their chemical composition would be extremely useful, but it has yet to be achieved. In this paper, the performance of three nickel-based single crystal superalloys are considered; these are prototypes which might find future application in the industrial gas turbines used for electricity generation. Whilst these alloys are shown to be Al_2O_3 formers, they are marginally so and this has allowed the factors influencing Al_2O_3 formation to be studied in detail.

Experimental procedures

Casting and Heat treatment. The prototype nickel-based single crystal superalloy SCA425+ was chosen for the present work. This a candidate for future application in industrial gas turbines partly on account of its Cr content (15.5 wt.%) which is appreciably greater than for most other single crystal alloys – many of which were designed for aeroengine applications. Two derivatives of SCA425+ containing 0.25 and 0.5 wt.% Si are also studied here; it has been reported that Si is beneficial with regard to Al_2O_3 layer formation [1-3], but one purpose of the experimentation was to check this for the SCA425+ alloy. The nominal compositions of the three alloys investigated are given in Table 1.

An industrial scale investment casting facility at the University of Birmingham was used to prepare single crystal castings in the form of 15 mm diameter rods of length 150 mm. Typically,

Table1 Nominal compositions ([wt.%], Ni-bal) of superalloys investigated.

	Co	Cr	Mo	W	Al	Ta	Hf	Si
SCA425+	5.0	15.5	1.0	4.0	4.55	8.0	0.1	-
SCA425+0.25Si	5.0	15.5	1.0	4.0	4.55	8.0	0.1	0.25
SCA425+0.5Si	5.0	15.5	1.0	4.0	4.55	8.0	0.1	0.5

This article is an open access article under the terms and conditions of the Creative Commons Attribution (CC BY) license (https://creativecommons.org/licenses/by/4.0)

three rods were cast in each run with a withdrawal speed of ~200 mm per hour; the anticipated temperature gradient was 7.5ºC/mm. Ceramic moulds were prepared from alumina, silica and zircon in the usual way; the final mould thickness was ~6 mm. These were de-waxed in a steam autoclave for 5 mins and then sintered at 1000°C for an hour in air, prior to casting. The casting stock was melted by Ross & Catherall in Sheffield, UK to industry-leading standards. Chemical analysis indicated less than 7.2 ppmw of sulfur in the stock, so that – since the oxidation temperatures used here are 1000ºC or lower and the tests carried out isothermally – any influence of this element on oxidation performance will be negligible [4]. Casting was carried out under a vacuum of better than 10^{-4} Pa. The single crystal bars were carefully removed from the mould, and then sand blasted. In order to confirm whether the cast bar contains any grain defect, the bars were macro etched using HCl + 5~10 vol.% H_2O_2 solution. No freckles were observed. Subsequently, the castings were heat treated to remove chemical heterogeneity inherited from the processing, and to develop appropriate precipitate morphologies. The solution treatment chosen for SCA425+ was 1280ºC 1 hour →1300ºC 5 hours, followed by air-cooling; for SCA425+0.25Si, it was 1260ºC 1 hour →1280ºC 5 hours, followed by air-cooling; for SCA425+0.5Si, it was 1230ºC 1 hour →1250ºC 5 hours, followed by air-cooling. The first and second aging treatments for all alloys were 1120°C 24 hours and 850°C 20 hours followed by air-cooling, respectively.

Oxidation test. 2 mm thick discs were sliced from the heat-treated castings, polished to 0.05μm alumina and cleaned, and then placed in an Al_2O_3 boat before being exposed isothermally at 900ºC, 950ºC and 1000ºC for 100 hours, respectively. The oxidized surfaces were subjected to X-ray diffraction (XRD) analysis. Cross-sections of these samples were analysed using back-scattered electron (BSE) imaging in a scanning electron microscope (SEM) equipped with energy dispersive X-ray spectroscopy (EDX).

Modelling. In order to predict the growth rate of Al_2O_3 on any given Ni-base superalloy, separate thermodynamic and kinetic factors are proposed. The details will be discussed elsewhere [5], but briefly the oxidation rate of n-type Al_2O_3, k_t, can be estimated according to

$$k_t \propto \left[\sum_{n=i}\left(z_i - z_{\mathrm{Al}}\right)c_i^{\gamma}\right]\cdot \Delta G_f \tag{1}$$

where z_i is the valence of element i's ion: for examples, when i = Ni, then z_{Ni} = (valence of Ni in the most stable nickel oxide, NiO) = 2 and z_{Al} is the valence of Al ion = 3. c_i^{γ} represents the atomic fraction of element i in the γ phase at the oxidation temperature. Thus the square brackets term in Eq.1 represents total effective valence in Al_2O_3 ($\mathrm{Val}_t^{\mathrm{eff}}$). Here, ΔG_f is the Gibbs free energy of formation of the Al_2O_3 oxide and this can be expanded consistent with the Van't Hoff isotherm [6, 7] according to

$$\Delta G_f = \Delta G_0 + RT\ln\left(\frac{a_{\mathrm{Al_2O_3}}^{2/3}}{a_{\mathrm{Al}}^{4/3}\cdot P_{\mathrm{O_2}}}\right) \tag{2}$$

where ΔG_0 is the standard free energy of formation per 1 mol of O_2, which can be calculated as 0.2193×T-1127.3137 kJ/mol [8], T is absolute temperature and R is the gas constant. The activity of the oxide of Al is represented by $a_{\mathrm{Al_2O_3}}$ (this is commonly taken to be unity) and a_{Al} is the activity of Al in the nickel-base superalloy which is subject to oxidation. The partial pressure of oxygen is $P_{\mathrm{O_2}}$ which is 0.21 atm in one of atmosphere air.

Results and Discussion

Isothermal Oxidation Testing. In Fig.1, SEM micrographs of the oxidized superalloys are shown after exposure at temperatures of 900ºC, 950ºC and 1000ºC for 100 hours. The EDX analysis (Fig.2) revealed that the darkest oxide layer in Fig.1 consisted mainly of aluminium and oxygen, consistent with α-Al_2O_3; the presence of this phase was confirmed by XRD. One can see from Fig.1

that there is a tendency for α-Al_2O_3 to form a continuous layer only at higher Si contents and when the exposure temperature is higher; at lower temperatures and in the absence of Si, internal oxidation is prevalent. Additionally, the presence of Ta_2O_5/$NiTa_2O_6$ and Cr_2O_3 were confirmed by both EDX and XRD. For example, it was found that Ta_2O_5 is the brightest oxide and Cr_2O_3 is the second brightest oxide for SCA425+ exposed to 1000ºC, and $NiTa_2O_6$ is the brightest oxide and Cr_2O_3 is the second brightest oxide for the same alloy at 900ºC. Thus, as one moves outward across the scale towards the outer surface, one moves from Al_2O_3 → Ta_2O_5/$NiTa_2O_6$→ Cr_2O_3. A continuous Al_2O_3 layer is prevalent at higher temperature and when Si is added.

Fig.3 indicates the thicknesses of Al_2O_3, Ta_2O_5 and Cr_2O_3 with respect to the Si content in the alloys exposed at 1000ºC for 100 hours. No significant changes in the thickness of Al_2O_3 were observed with respect to Si content. On the contrary, the more Si is added, the thinner Cr_2O_3 and Ta_2O_5 become. Furthermore, it is obvious from Fig.1 that the Al_2O_3 sub-scale becomes a perfect Al_2O_3 layer with Si addition. This implies quicker decreases of P_{O_2} at Ta_2O_5/Al_2O_3 interface when Si is present. In other words, Si promotes the formation of a protective Al_2O_3 layer.

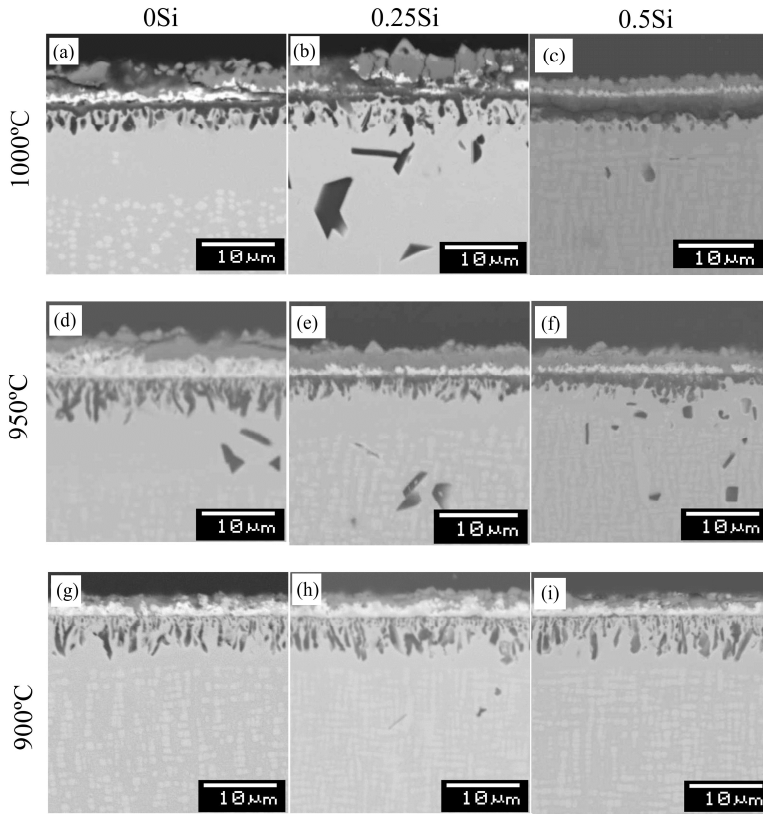

Fig.1 Micrographs of cross-sectioned superalloys after 100 hours exposure in one atmosphere air. Note that all micrographs were obtained from the dendrite core region of matrix.

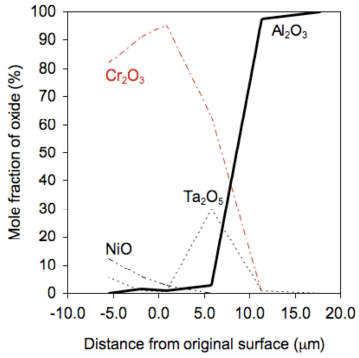

Fig.2 SEM-EDX result of Fig.1(a) stoichiometrically.

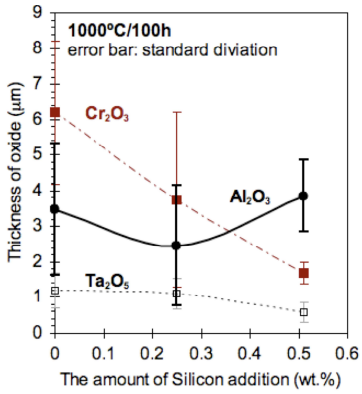

Fig.3 Summary of thickness of oxides in Fig.1 (a), (b) and (c).

Microsegregation Analysis. In order to rationalise the oxidation behaviour of the various chemical composition, microsegregation in the matrix was analyzed through the dendrite structure. Even when Si is added, SCA425+ could not form a continuous Al_2O_3 layer at 900ºC, see Fig.1; therefore rougher-surfaced (120 grit) [9] longer-exposed samples were used for this purpose. By simultaneously analyzing both (i) from where the Al_2O_3 becomes continuous/discontinuous, and (ii) how much difference exists in the chemical composition through the dendrite structure, Fig.4 was prepared. The chemical compositions of superalloys were analyzed at about 100 μm inwards from metal/oxide interface along the [001] direction to avoid the effect of oxidation. The chemical composition in Fig.4 indicates the average composition over about 300μm^2. As the dendrites were

tilted, these angles were measured by using BSE image contrast, and used geometrically to calibrate when the (ii) composition was compared with (i) the position. Fig.4 represents the relationship between the composition difference due to microsegregation and Al_2O_3 morphology. It is obvious from Fig.4a that the discontinuous Al_2O_3 preferentially formed at dendrite core region due to the microsegregation of W and Ta. Note that these compositions will be used for modelling in the next chapter.

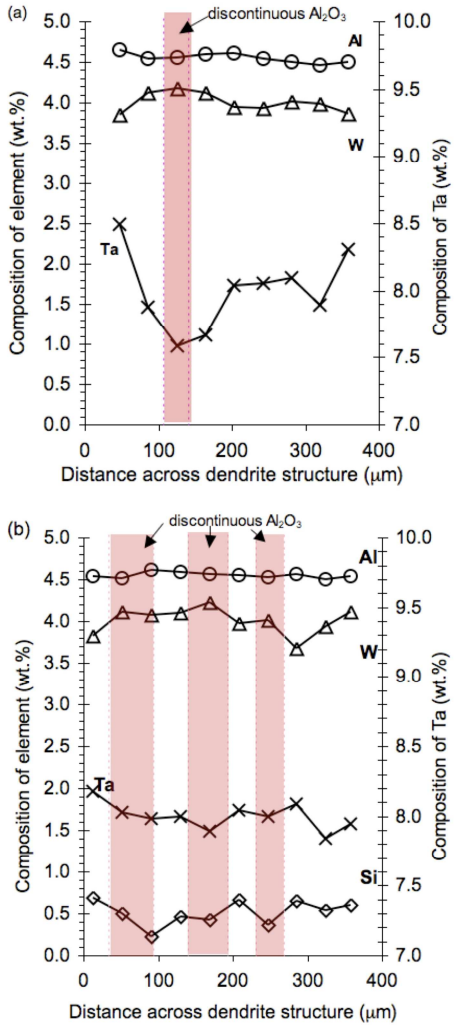

Fig.4 Microsegregations in matrix and Al_2O_3 morphologies at surface of (a) SCA425+ exposed at 1000ºC for 300 hours, and (b) SCA425+0.5Si exposed at 900ºC for 300 hours.

Oxidation diagram. Inspired by the form of Eq.1, so-called oxidation diagrams can now be developed. As will be seen, these have some power for the prediction of oxidation performance and therefore are useful for alloy design purposes. Fig 5 represents the oxidation diagram calculated from the microsegregation result above; on the x- and y-axes are plotted estimates of Val_t^{eff} and ΔG_f, respectively. Alloys which form Al_2O_3 readily are expected to lie towards the bottom left of the diagrams; those for which a continuous Al_2O_3 scale is unlikely towards the top right. Since the performance of SCA425+ has been shown to be marginal with regard to continuous Al_2O_3 scale formation, its composition can be used to calibrate Eq.1 and thus to identify the location of a critical isocontour; the isocontours tend asymptotically to the two axes owing to its hyperbolic nature, but in practice it has been found that the curvature is rather gentle in the calculated regimes of interest. These have been done for the temperatures 900ºC and 1000ºC on the diagrams given in Fig 5. Thus the calculated line which is plotted passes through the point for SCA425+. Fig.5 also contains the calculated results of some well-known superalloys – chemical compositions are given in [10] – for which the oxide morphologies have been reported in the literature [10-15]. Note that there is some subjectivity involved in deciding whether any given alloy does indeed form a continuous layer of Al_2O_3, owing to the different practices used in the oxidation testing and the details reported; however one can see that the alloys which perform adequately tend to lie below the calculated line, and those not performing well lie above it. The sole discrepancy

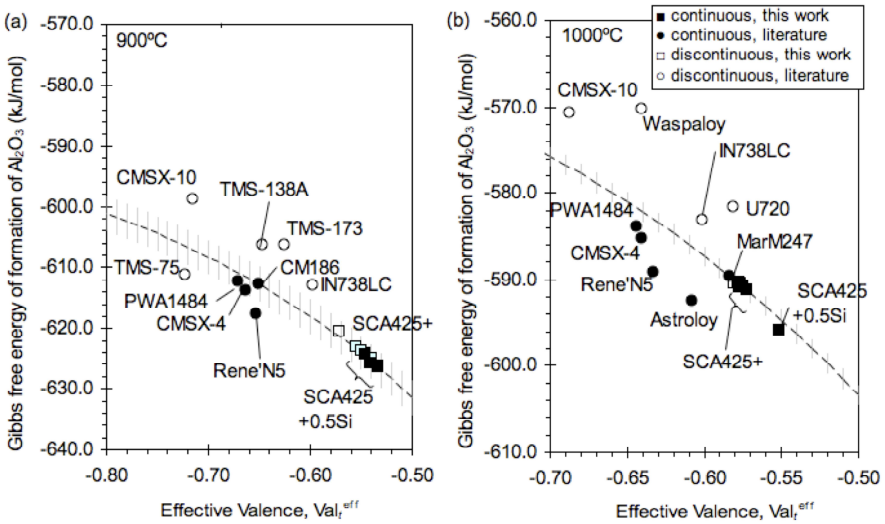

Fig.5 The thresholds of Al_2O_3 layer formation at (a) 900ºC and (b) 1000ºC in terms of Gibbs free energy of Al_2O_3 formation and total effective valence in Al_2O_3 index. Comparisons from the literatures [10-15].

found concerns the result for the TMS-75 alloy exposed at 900ºC for 100 hours. Our calculation predicted that TMS-75 is capable to form a continuous Al_2O_3, but report [14] indicates that it cannot, and reasons for this might be as follows. It is known that in the early (transient) stages of oxidation – before the steady-state is reached – a continuous layer of Al_2O_3 might not yet have become established. Furthermore, our attention has been restricted to the formation of n-type Al_2O_3, so that the cations are assumed to move more slowly than the anions. This is not necessarily the case for the transient θ-Al_2O_3 which can form in these systems at early stages [16].

The model can be used to estimate the sensitivity of continuous alumina scale formation to the chemical composition of any given superalloy in the following way. Starting with the baseline composition of SCA425+ consistent with the emphasis of this paper, calculations of ΔG_f and Val_t^{eff} have been made after systematically altering the mean chemical composition by 1at.% for each of the important alloying additions. The results can depicted on the oxidation diagrams, with vectors identifying the changes in position of the alloy with respect to the critical isocontour for continuous Al_2O_3 formation. Our predictions are as follows, see Fig.6. First of all, in general, the additions of Al and Si are beneficial to form Al_2O_3 layer. Secondly, Cr, Re and Co are slightly beneficial or neutral. On the contrary, the addition of W, Ta, Nb, Ru, Ti and Mo are considered to be detrimental.

It can also be noticed from Fig.6 that Si addition and Al addition has very similar vectors. First of all, both Al and Si have similar beneficial effect on SCA425+ thermodynamically: +1at.%Al decrease ΔG_f from -620.45 kJ/mol to -624.91 kJ/mol and +1at.%Si to -624.99 kJ/mol. Thus, there is little difference in y- axes between +1at.%Al and +1at.%Si in Fig.6. In order to understand the small difference in x- axes between them, the factor influencing total effective valence of SCA425+ alloy are summarised in Fig.7. Here, adding higher valence element (Si^{4+} etc…) and/or removing lower valence element (Ni^{2+} etc…) from matrix increase total effective valence in Al_2O_3. Note that increasing effective valence is detrimental. In Al addition in Fig.7, there is a significant increase of the total effective valence due to the increases of volume fraction of γ' phase (Vf). This is because increasing Vf causes the reduction of Ni content from both γ/γ' phase (Again, Ni has the valence of positive 2 in NiO). In Si addition, there is also a small effect of Vf increase, but this effect is much smaller than that of Al addition above. Instead, there is a significant effect of adding higher valence element, as Si has the valence of positive 4 in SiO_2. Therefore, despite the fact that Si has the valence of positive 4, as Si addition does not significantly increase Vf than Al addition, both Al and Si shows similar effect on total effective valence in Al_2O_3 in Fig.6.

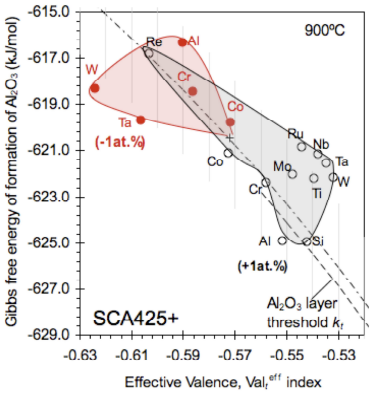

Fig.6 The effect of alloying element has on the oxidation diagram of at 900ºC

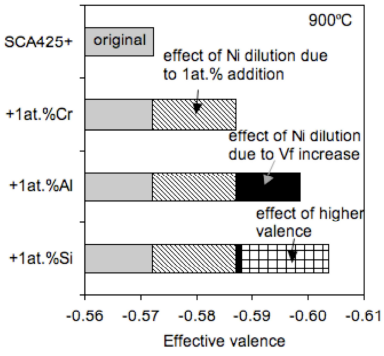

Fig.7 The effect of Cr, Al and Si on the effective valence of SCA425+ alloy at 900ºC

Summary

The SCA425+ single crystal superalloy is an alumina-former but only marginally so; higher oxidation temperatures and additions of Si promote the formation of a continuous layer of alumina. When estimates are made for effective valence and the thermodynamic driving force for the formation of Al_2O_3, the concept of an oxidation diagram can be used to predict whether any given alloy is likely to be an α-Al_2O_3 former. It can be considered that Si addition is similarly beneficial like Al addition due to its positive thermodynamical effect and less increase of Vf.

Acknowledgements

The authors are grateful to Siemens Industrial Turbomachinery AB for sponsoring this work. The invaluable advice and full support of Prof. Hugh E. Evans, Dr. Mary P. Taylor, Dr. Yu-Lung Chiu, Dr. Robert Broomfield and Mr. Peter Cranmer at the University of Birmingham is acknowledged.

References

[1] R.V. Miner and C.E. Lowell: *Effects of Silicon Additions on Oxidation and Mechanical Behavior of the Nickel-Base Superalloy B-1900*. (NASA, U.S. 1975).

[2] A. Sato, H. Harada, J. Ang, Y. Koizumi, T. Kobayashi, K. Kawagishi and H. Imai, in: *Vol.53 of Materials for Advanced Power Engineering 2006 Proceedings of the 8th Liége Conference Part 1,*edited by J. Lecomte-Beckers, M. Carton, F. Schubert, P.J. Ennis. Schriften des Forschungszentrums Jülich, Reihe Energietechnik/ Energy Technology, (2006), p.655

[3] A.C. Yeh, K. Kawagishi, H. Harada, T. Yokokawa, Y. Koizumi, T. Kobayashi, J. Ping, J. Fujioka and T. Suzuki, in: *Superalloys2008*, edited by R.C. Reed, K.A. Green, P. Caron, T.P. Gabb, M.G. Fahrmann, E.S. Huron, S.R. Woodard, TMS, (2008), p.619

[4] J.L. Smialek, C.A. Barrett and J.C. Schaeffer: Materials Selection and Design, Vol. 20. edited by G.E Dieter. ASM International, (1997), p.589

[5] A. Sato, Y.L. Chiu and R.C. Reed: submitted to Acta Materialia (2010)

[6] N. Birks, G.H. Meier and F.S. Pettit: *Introduction to the high-temperature oxidation of metals*. Cambridge University Press, (2006).

[7] N. Saunders and A.P. Miodownik: *CALPHAD Calculation of Phase Diagrams -A Comprehensive Guide-*. edited by R.W.Cahn. PERGAMON MATERIALS SERIES, Vol. 1. PERGAMON, (1998).

[8] O. Knacke, O. Kubaschewski and K. Hesselmann: *Thermochemical properties of Inoganic substances.* edited by O. Knacke, O. Kubaschewski, K. Hesselmann. Springer-Verlag Berlin, Heidelberg, (1991).

[9] N. Birks, G.H. Meier and F.S. Pettit: JOM Vol. 46 (1994), p.42

[10] R.C. Reed: *The Superalloys -fundamentals and applications-*. Cambridge University Press, (2006).

[11] M. Göbel, A.Rahmel and M. Schütze: Oxid. Met. Vol.39 (1993), p.231

[12] G.H. Meier, F.S. Pettit and K. Onal: *Interaction of Steam/Air Mixtures With Turbine Airfoil Alloys and Coatings Final Report.* US Department of Energy, Morgantown Energy Technology Center, Contract Number DE-FE21-92MC29061, (2002)

[13] K. Onal, M.C. Maris-Sida, G.H. Meier and F.S. Pettit, in: *Superalloys2004* edited by K.A. Green, T.M. Pollock, H. Harada, T.E. Howson, R.C. Reed, J.J. Schirra, S. Walston. TMS, (2004), p.607

[14] K. Kawagishi, A. Sato, T. Kobayashi and H. Harada: J. Japan Inst. Metals Vol.71 (2007), p.313

[15] J.H. Chen, P.M. Rogers and J.A. Little: Oxid. Met. Vol.47 (1996), p.381

[16] B.A. Pint, J.R. Martin and L.W. Hobbs: Solid State Ionics Vol.78 (1995), p.99